9-1-2017

Direct Numerical Simulation of Turbulent Katabatic Slope Flows with an Immersed-Boundary Method

Clancy Umphrey
Boise State University

Ray DeLeon
Boise State University

Inanc Senocak
Boise State University

Boundary-layer Meteorology manuscript No.
(will be inserted by the editor)

# of Turbulent Katabatic Slope Flows with an Immersed-Boundary Method

Clancy Umphrey[1] · **Rey DeLeon**[1,2] · **Inanc Senocak**[1]

Received: DD August 2016 / Accepted: DD Month YEAR

Abstract We investigate a Cartesian-mesh immersed-boundary formulation within an incompressible flow solver to simulate laminar and turbulent katabatic slope flows. As a proof-of-concept study, we consider four different immersed-boundary reconstruction schemes for imposing a Neumann-type boundary condition on the buoyancy field. Prandtl's laminar solution is used to demonstrate the second-order accuracy of the numerical solutions globally. Direct numerical simulation of a turbulent katabatic flow is then performed to investigate the applicability of the proposed schemes in the turbulent regime by analyzing both first- and second-order statistics of turbulence. First-order statistics show that turbulent katabatic flow simulations are noticeably sensitive to the specifics of the immersed-boundary formulation. We find reconstruction schemes that work well in the laminar regime may not perform as well when applied to a turbulent regime. Our proposed immersed-boundary reconstruction scheme agrees closely with the terrain-fitted reference solutions in both flow regimes.

Keywords Direct numerical simulation · Immersed-boundary method · Katabatic flows · Stable stratification · Turbulence

1 Introduction

Turbulent katabatic flows with stable stratification commonly occur in the atmospheric boundary layer with important implications for weather forecasting, air pollution and wind-energy applications. The subject has been the focus of several numerical and experimental investigations aimed at establishing a better understanding of the underlying flow physics (Mahrt, 2014).

Inanc Senocak
senocak@boisestate.edu

[1] Boise State University, Boise, ID, USA
[2] University of Idaho, Moscow, ID, USA

Skyllingstad (2003) conducted large-eddy simulations (LES) of katabatic flows to demonstrate the effect of terrain-slope changes on drainage winds, which can hinder the formation of very stable regimes. Cuxart et al. (2007) carried out mesoscale simulations of the flow over an island in the Mediterranean to study the interaction of different scales of motion at night. Papadopoulos and Helmis (1999) investigated the evening and morning transition of katabatic slope flows experimentally and elucidated the processes involved in their formation and destruction. Mahrt (2016) studied stably stratified flow in a shallow valley experimentally, and identified oscillations within the valley with a period of 10 min. Shapiro and Fedorovich (2007) considered the inhomogeneity of sloping surfaces by developing an analytical model in which buoyancy varied linearly down the slope, which are physical processes not accounted for in Prandtl's laminar solution (Prandtl, 1942).

As the numerous physical processes involved in katabatic flow over complex terrain with heterogeneous surface conditions (Mahrt, 2014) make it difficult to unravel their interplay without introducing certain simplifications, an inclined, homogeneous flat-terrain flow serves as an idealized test case to develop a fundamental understanding of katabatic flows. An inclined flat surface is also a realistic simplification for the study of katabatic flows in the Great Plains of the U.S.A and Antarctica (Parish and Waight III, 1987). Equally important are slope flows over homogeneous surfaces, which serve as a canonical test case for validating new numerical methods and physical models.

We evaluate and refine here an immersed-boundary approach for katabatic slope flows. The immersed-boundary method is an attractive approach for representing complex geometry on a Cartesian mesh without the need for a manual mesh generation. The simplicity of the Cartesian formulation also eases computational parallelization of the flow solver. The method, which was pioneered by Peskin (1972), traces its origins to the numerical simulation of blood flow through the heart. The immersed-boundary method immerses a predefined geometry inside a Cartesian mesh and imposes surface boundary conditions on the nodes of the intersected cells using either a forcing function or a reconstruction scheme. While the immersed-boundary method has been an active area of research in computational fluid dynamics for engineering applications, it has also been proposed as an alternative meshing approach for geophysical flows (Tseng and Ferziger, 2003; Senocak et al., 2004; Smolarkiewicz et al., 2007).

Various approaches have been proposed to implement the immersed-boundary method (Mittal and Iaccarino, 2005; Sotiropoulos and Yang, 2014). Despite the importance of heat transfer in many engineering or geophysical flows, the majority of studies have focused on velocity boundary conditions, with little consideration given to the boundary conditions related to scalar transport. Boundary conditions can be imposed as Dirichlet (i.e. prescribed temperature), Neumann (i.e. prescribed heat flux) or a mixed type. Reconstruction schemes developed for velocity boundary conditions may be applied to impose a prescribed temperature boundary condition. However, few studies focus on the implementation of Neumann-type boundary conditions within an

immersed-boundary formulation. Pacheco-Vega et al. (2007) describe a generalized immersed-boundary approach applicable to both the Dirichlet- and Neumann-type boundary conditions. For the Neumann type, a numerical stencil is generated around a surface point requiring the Neumann boundary condition, whereby the stencil is not necessarily aligned with the numerical stencils on the Cartesian grid. Therefore, linear and bilinear interpolations are used to bring neighbouring values onto the imposed numerical stencil before calculating the Neumann boundary condition. Zhang et al. (2008) use a feedback-forcing type immersed-boundary method, whereby values at neighbouring grid points are interpolated to a surface point to determine heat transfer from the surface of a cylinder. Kang et al. (2009) performed a direct numerical simulation (DNS) of conjugate heat transfer consisting of a solid cylinder in a channel flow with a heated bottom plane using the immersed-boundary reconstruction found in Fadlun et al. (2000). A Dirichlet-type boundary condition was imposed for the temperature field by linearly interpolating the temperature within the solid to the fluid boundary. A Neumann boundary condition for temperature was satisfied by a one-sided finite difference in the fluid domain.

Our chief objective here is to develop an immersed-boundary reconstruction scheme for imposing a Neumann-type boundary condition on the buoyancy field, and to assess its performance in both laminar and turbulent flows. To date, a consistent performance for both types of flow has not been assessed. We consider an idealized katabatic flow above an inclined surface as a canonical problem. While an immersed-boundary method does not provide any obvious advantage over a body-fitted mesh for simulating a flow over a flat surface, an idealized slope flow establishes a benchmark case able to be simulated with a body-fitted approach, from which one may assess the formal accuracy of reconstruction schemes, including the performance in calculating both laminar and turbulent flows.

2 Numerical Formulation

Cartesian grid nodes do not generally coincide with the immersed geometry or terrain. Therefore, a challenge for the immersed-boundary method is to indirectly enforce the boundary conditions on the discretized form of the governing equations. The original immersed-boundary method introduced a body-force term to the momentum equations (Peskin, 1972), which worked well for elastic surfaces, but suffered from limited numerical stability in general. Mohd-Yusof (1997) proposed the *direct-forcing* approach that alleviated numerical stability constraints by indirectly incorporating a body force term, F_i, into the discretized form of the momentum equations as

$$\frac{u_i^{n+1} - u_i^n}{\Delta t} = RHS_i + F_i, \tag{1}$$

where RHS_i includes advective, diffusive, and pressure gradient terms. If the velocity at the boundary can be prescribed as $u_i^{n+1} = V_i$ for all n, then the

body force becomes

$$F_i = -RHS_i + \frac{V_i - u_i^n}{\Delta t} \tag{2}$$

from Eq. 1. By substituting Eq. 2 into Eq. 1, the body force is implicitly included by prescribing the velocity field, V_i. As the Cartesian grid is not coincident with the immersed surface, a reconstruction scheme is required to impose the boundary conditions on the Cartesian nodes near the surface, which in turn become boundary conditions for the rest of the flow.

We adopt the GIN3D flow solver (see Thibault and Senocak, 2012; Jacobsen and Senocak, 2011, 2013; DeLeon et al., 2013, for details), in which an immersed-boundary method based on the aforementioned direct-forcing approach is implemented for the velocity field (DeLeon et al., 2012). A separate geometric preprocessor is available to immerse an arbitrarily complex geometry into a Cartesian grid (Senocak et al., 2015). In the GIN3D solver, the velocity reconstruction scheme for laminar conditions follows a linear approach in the direction normal to the surface, similar to the works of Gilmanov et al. (2003), Gilmanov and Sotiropoulos (2005) and Gilmanov and Acharya (2008). In wall-resolved LES of turbulent flows in which the viscous sublayer is resolved, the same linear reconstruction schemes may be used, albeit at modest Reynolds numbers and with a high computational cost. However, for wall-modelled LES, the linear reconstruction of the no-slip boundary condition is inadequate because the spatial resolution is too coarse to resolve any part of the viscous sublayer. In those cases, the GIN3D solver adopts the logarithmic reconstruction scheme proposed by Senocak et al. (2004) along with a subgrid-scale model (Senocak et al., 2007) consistent with the logarithmic law-of-the-wall theory (Pope, 2000).

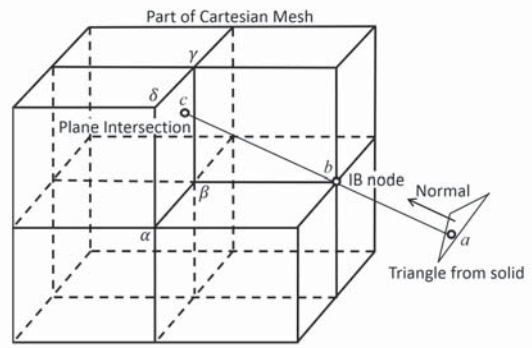

Fig. 1 Sketch of the general indirect boundary reconstruction scheme at an immersed-boundary node by projecting a line in the normal direction from the nearest triangular element of the boundary into the fluid domain.

Figure 1 illustrates the implementation of the boundary-reconstruction scheme. A line in the normal direction from the nearest triangular element of

the immersed boundary (point a) is projected through the immersed-boundary node, which is defined as the nearest fluid node to the surface (point b), and onto a Cartesian cell face within the fluid domain (point c). This line will be referred to as the immersed-boundary line. Values at a are known as prescribed boundary conditions and values at c are reconstructed by bilinear interpolation from the neighbouring Cartesian grid nodes marked by the Greek letters α, β, γ, and δ. In the case of linear velocity reconstruction, another linear interpolation along the immersed-boundary line between a and c is performed to overwrite the current value at b. We emphasize that a linear reconstruction for velocity is appropriate for the present problem because the simulation resolves the flow field down to the surface.

3 Buoyancy Reconstruction Schemes

We investigate four reconstruction schemes for imposing Neumann-type boundary conditions in the context of a direct-forcing immersed-boundary approach. The buoyancy term is conveniently solved by imposing the boundary conditions for katabatic slope flows. Following the work of Fedorovich and Shapiro (2009), we prescribe a constant buoyancy flux at the surface to establish a canonical test case for both laminar and turbulent flows. While a constant surface buoyancy flux may not be ideal for studying the physics of actual katabatic flows over sloped terrain, it serves our present purposes well. A spatially-varying surface-buoyancy flux (Shapiro and Fedorovich, 2007) may also be considered.

Scheme 1 makes use of the buoyancy-gradient boundary condition at the surface and buoyancy-gradient in the fluid node calculated with a central-difference. These two data points are then used to calculate the buoyancy at the immersed-boundary node. Gilmanov et al. (2003) proposed this approach to impose a Neumann-type boundary condition on the pressure field for an incompressible solution, but did not test for the transport of a generic scalar field. Scheme 1 is outlined in the following steps for a general scalar ϕ with the help of Fig. 1:

1. Calculate $\left(\frac{\partial \phi}{\partial x_i}\right)$ at α-β-γ-δ in all three Cartesian coordinates ($i = 1, 2, 3$).
2. Linear interpolate these to c to obtain $\left(\frac{\partial \phi}{\partial x_i}\right)_c$.
3. The normal gradient of ϕ at c becomes
$$\left(\frac{\partial \phi}{\partial n}\right)_c = \mathbf{n}_a \cdot (\nabla \phi)_c \,, \tag{3}$$
where $\mathbf{n}_a$ is the surface normal vector at a.
4. With the normal ϕ gradient boundary condition at the surface, $\left(\frac{\partial \phi}{\partial n}\right)_a$, and the known normal ϕ gradient at c, $\left(\frac{\partial \phi}{\partial n}\right)_c$, linear interpolate along the immersed-boundary line to the midpoint between b and c to determine $\left(\frac{\partial \phi}{\partial n}\right)_{bc}$.

5. Linearly interpolate to bring ϕ from α-β-γ-δ to c, giving ϕ_c.
6. The value of ϕ at the immersed-boundary node is then calculated using a central-difference approximation

$$\phi_b = \phi_c - \Delta s_{bc} \left(\frac{\partial \phi}{\partial n} \right)_{bc}, \tag{4}$$

where Δs_{bc} is the distance along the immersed-boundary line from b to c.

In step 1, Gilmanov et al. (2003) does not mention a method for calculating the first derivatives, so we approximate those derivatives with a second-order accurate central difference, because the scheme was originally applied to the pressure field. The central difference for computing the first derivative of ϕ with respect to z is written as

$$\left(\frac{\partial \phi}{\partial z} \right)_k = \frac{\phi_{k+1} - \phi_{k-1}}{2\Delta z}, \tag{5}$$

where k represents the grid index, and Δz is the uniform mesh spacing in the z direction. We note that scheme 1 has not been validated for the transport of a generic scalar field. The remaining reconstruction schemes are unique to our work to the best of our knowledge. In designing these reconstruction schemes, we devote special attention to include only computational cells that are not intersected by the immersed boundary to avoid including unreconstructed values at the immersed-boundary node. We find that this subtle issue, which is not addressed in scheme 1, is important.

Scheme 2 assumes the ϕ gradient along the immersed-boundary line from a to c is constant. Analogous to Eq. 4, a central difference using the ϕ gradient boundary condition is used to calculate the buoyancy at the immersed-boundary node,

$$\phi_b = \phi_c - \Delta s_{bc} \left(\frac{\partial \phi}{\partial n} \right)_a. \tag{6}$$

Scheme 3 is identical to scheme 1, except the first derivatives in step 1 are approximated with one-sided differences to avoid including immersed-boundary nodes in the reconstruction, because values at those nodes are yet to be updated and may otherwise introduce errors into the scheme. We use a second-order-accurate, one-sided difference formula (Tannehill et al., 1997), which can be written for a one-dimensional uniform mesh as

$$\left(\frac{\partial \phi}{\partial z} \right)_k = \frac{-3\phi_k + 4\phi_{k+1} - \phi_{k+2}}{2\Delta z}. \tag{7}$$

Scheme 4 adopts a nearest-neighbour interpolation to compute the ϕ gradient at point b. To calculate ϕ at the immersed-boundary node, a second-order-accurate, one-sided difference is used that includes the ϕ gradient at b and two cell face intersection points from the fluid side. This reconstruction requires an additional fluid point not shown in Fig. 1, referred to here as d,

where the immersed-boundary line intersects the next cell face after point c. Values of ϕ are brought to d through linear interpolation from neighbouring Cartesian grid points in the same way as values are brought to c through linear interpolation from α, β, γ, and δ. The reconstruction is performed by solving for ϕ_b in

$$\left(\frac{\partial\phi}{\partial n}\right)_b = \frac{-\phi_d\left(h_c-h_b\right)^2+\phi_c\left(h_d-h_b\right)^2-\phi_b[\left(h_d-h_b\right)^2-\left(h_c-h_b\right)^2]}{\left(h_c-h_b\right)\left(h_d-h_b\right)\left(h_d-h_c\right)}, \quad (8)$$

where h refers to the distance from the surface of each respective point b, c, and d. Equation 8 is the version of Eq. 7 for non-uniform grid spacing (Ferziger and Perić, 2012).

A fifth scheme was also proposed by Umphrey et al. (2016), who also combined our schemes with different velocity reconstruction schemes, but is not considered here for the sake of clarity.

4 Results

We simulate katabatic flows above an infinite plane inclined at an angle α to validate the aforementioned immersed-boundary reconstruction schemes, which impose a Neumann-type boundary condition for the buoyancy field. A one-dimensional model for laminar flow of a stratified fluid along a uniformly cooled or heated sloping plane was developed by Prandtl (1942). Figure 2 illustrates Prandtl's laminar solution for the case of a uniformly cooled sloping plane, where a katabatic flow develops with a low-level downslope jet topped by a weak upslope return flow. Both the velocity and buoyancy fields approach zero away from the surface. Fedorovich and Shapiro (Shapiro and Fedorovich, 2004; Fedorovich and Shapiro, 2009) published a non-dimensional form of Prandtls solution,

$$u_n = \sin(z_n/\sqrt{2})\exp(-z_n/\sqrt{2}), \quad (9)$$

$$b_n = \cos(z_n/\sqrt{2})\exp(-z_n/\sqrt{2}), \quad (10)$$

where

$$z_n = z\nu^{-1/2}N^{1/2}\sin^{1/2}\alpha, \quad (11)$$

$$u_n = u\nu^{1/2}N^{3/2}B_s^{-1}\sin^{1/2}\alpha, \quad (12)$$

$$b_n = b\nu^{1/2}N^{3/2}B_s^{-1}\sin^{1/2}\alpha. \quad (13)$$

Here, subscript n refers to normalized quantities, u is the velocity component parallel to the slope, z is the distance normal to the slope surface, b is buoyancy ($b = g\theta/\Theta_r$, where g is the gravitational acceleration, θ is the potential temperature perturbation, Θ_r is the reference potential temperature), ν is the kinematic viscosity equal to the thermal diffusivity, N is the Brunt-Väisälä (or buoyancy) frequency ($N^2 = (g/\Theta_r)\left(d\Theta_e/dz'\right)$, where Θ_e

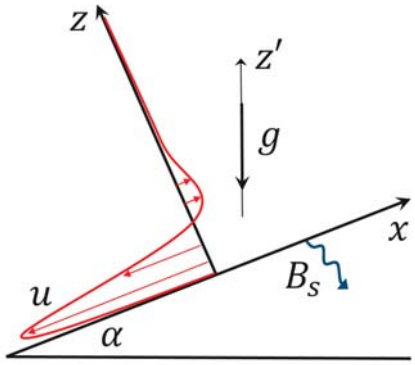

Fig. 2 Sketch of Prandtl's laminar solution of katabatic flow on an infinite plane for a constant surface buoyancy flux. Note that for the simulations, the gravity vector is rotated and a flat surface is considered.

is the environmental potential temperature), B_s is the surface buoyancy flux ($B_s = -\nu \left(db/dz\right)|_{z=0}$), and α is the slope angle. The analytical solution has as boundary conditions $u(0) = 0$, $\left(db_n/dz_n\right)|_{z_n=0} = -1$, and $u_n \to 0$, $b_n \to 0$ as $z_n \to \infty$. While the above analytical solution serves as an excellent benchmark to evaluate various numerical methods and to formalize the order of accuracy of numerical solutions, it does not guarantee success in the turbulent regime, as we show below.

It is common to include buoyancy effects in the incompressible Navier-Stokes equations through the Boussinesq approximation, which is valid when density variations are small and vary linearly with the temperature difference (Ferziger and Perić, 2012). Following the work of Fedorovich and Shapiro (2009), the momentum-balance equations for slope flow are

$$\frac{\partial u}{\partial t} + u\frac{\partial u}{\partial x} + v\frac{\partial u}{\partial y} + w\frac{\partial u}{\partial z} = -\frac{\partial p}{\partial x} + \nu\left(\frac{\partial^2 u}{\partial x^2} + \frac{\partial^2 u}{\partial y^2} + \frac{\partial^2 u}{\partial z^2}\right) + b\sin\alpha, \tag{14}$$

$$\frac{\partial v}{\partial t} + u\frac{\partial v}{\partial x} + v\frac{\partial v}{\partial y} + w\frac{\partial v}{\partial z} = -\frac{\partial p}{\partial y} + \nu\left(\frac{\partial^2 v}{\partial x^2} + \frac{\partial^2 v}{\partial y^2} + \frac{\partial^2 v}{\partial z^2}\right), \tag{15}$$

$$\frac{\partial w}{\partial t} + u\frac{\partial w}{\partial x} + v\frac{\partial w}{\partial y} + w\frac{\partial w}{\partial z} = -\frac{\partial p}{\partial z} + \nu\left(\frac{\partial^2 w}{\partial x^2} + \frac{\partial^2 w}{\partial y^2} + \frac{\partial^2 w}{\partial z^2}\right) + b\cos\alpha, \tag{16}$$

and for convenience, the heat-balance equation is written in terms of buoyancy,

$$\frac{\partial b}{\partial t} + u\frac{\partial b}{\partial x} + v\frac{\partial b}{\partial y} + w\frac{\partial b}{\partial z} = \nu\left(\frac{\partial^2 b}{\partial x^2} + \frac{\partial^2 b}{\partial y^2} + \frac{\partial^2 b}{\partial z^2}\right) - N^2\left(u\sin\alpha + w\cos\alpha\right). \tag{17}$$

Table 1 Simulation parameters for both laminar and turbulent katabatic slope flows.

Quantity	Symbol (Units)	Laminar Value	Turbulent Value
Slope angle	α (degrees)	30	60
Surface buoyancy flux	B_s (m^2 s^{-3})	-0.005	-0.5
Brunt-Väisälä frequency	N (s^{-1})	1	1
Kinematic viscosity	ν (m^2 s^{-1})	0.0005	0.0001
Thermal diffusivity	γ (m^2 s^{-1})	0.0005	0.0001

Here, u, v, and w are velocity components in the upslope, cross-slope, and slope-normal directions, respectively, p is the pressure, $b\sin\alpha$ and $b\cos\alpha$ are the buoyancy forcing terms, and the Prandtl number is assumed to be unity.

4.1 Laminar Katabatic Flow Simulation

We adopt the non-dimensional form of Prandtl's laminar solution to assess four different immersed-boundary reconstruction schemes for the simulation of the flow over an infinite flat plate with an angle of $\alpha = 30^\circ$ to the horizontal. To establish a body-fitted solution within a Cartesian flow solver, the gravity vector, instead of the horizontal surface, is rotated according to the slope angle. The flat plate is placed at the bottom of the domain such that immersed-boundary Cartesian scalar nodes (on a staggered grid) are 0.25Δ above the flat plate, where Δ is the uniform grid spacing. The domain height in the z-direction is $H = 1.27$ m. The no-slip condition and a constant buoyancy flux are enforced at the immersed surface, while the top of the domain is subject to the free-slip condition for the velocity and zero-flux conditions for buoyancy. Lateral boundaries are assumed to be periodic. The relevant simulation parameters are presented in Table 1. Three mesh spacings (Δ) are used throughout the laminar katabatic slope study: 0.005 m, 0.0025 m, 0.00125 m.

Figure 3 compares the normalized downslope velocity for the schemes discussed in Sect. 3 using a mesh spacing of $\Delta = 0.005$ m. While schemes 2–4 agree very well with the analytical solution, scheme 1 as proposed by Gilmanov et al. (2003) clearly underestimates the peak velocity of the low-level jet. In step 1 of scheme 1, the buoyancy gradient is approximated in the slope-normal direction of the fluid domain using a central-difference stencil that includes the immersed-boundary node. This is problematic, as the immersed-boundary node needs to be reconstructed before it can be used in a stencil. Scheme 3 resolves this issue by using a second-order-accurate, one-sided, finite-difference scheme, which neglects the immersed-boundary node. Central differences are still used in directions parallel to the slope as those stencils do not consider immersed-boundary nodes.

Figure 4 shows the normalized buoyancy produced by the same schemes compared with the analytical solution. While discrepancies in the calculation of buoyancy are less apparent, scheme 1 calculates a lower buoyancy near the surface compared with the benchmark solution. Based on these results, we exclude scheme 1 from the rest of the present study.

A grid-convergence study is often performed to identify the formal accuracy of a numerical solution. In computational analysis, a globally second-order-accurate solution is desirable at a minimum. To this end, we investigate the order of accuracy of scheme 4 using three systematically refined grids as shown in Fig. 5. As expected from an L_∞ norm of numerical error, first-order accuracy is achieved locally at the immersed-boundary node. However, the global solution is second-order accurate as evident by the slopes of the L_1 and L_2 norms. The formal accuracy of schemes 2 and 3 was also studied in Umphrey et al. (2016), with the same outcome as scheme 4. Note that we do not expect an order of accuracy higher than two, because the baseline flow solver adopts second-order numerics in time and space.

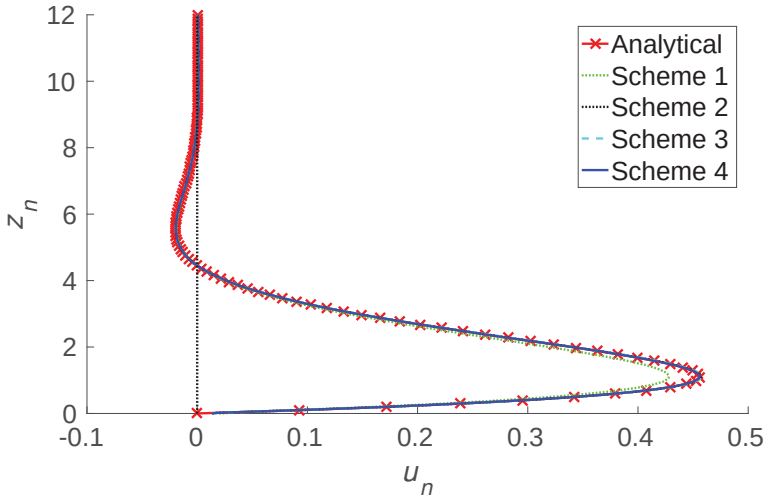

Fig. 3 Normalized downslope velocity component. Comparison of results from different buoyancy-reconstruction schemes with the analytical solution of the Prandtl model for laminar katabatic flow.

4.2 Turbulent Katabatic Flow, First-Order Statistics

Since reconstruction schemes that produce satisfactory results for laminar flows may not readily apply to turbulent flows, we consider Prandtl's model for turbulent katabatic slope flows. Because scheme 1 fails to reproduce Prandtl's laminar solution, we only consider schemes 2–4 in this section. Fedorovich and Shapiro (2009) performed DNS of idealized turbulent slope flows, in which they derived an integral slope-flow Reynolds number as $Re_I = |B_s|/\nu N^2 \sin\alpha$. Flows in which $Re_I > 3000$ are considered to have reasonably developed turbulence. For reference, the laminar simulation in Sect. 4.1 has $Re_I = 20$. The flat plate is once again placed at the bottom of the domain at 0.25Δ below

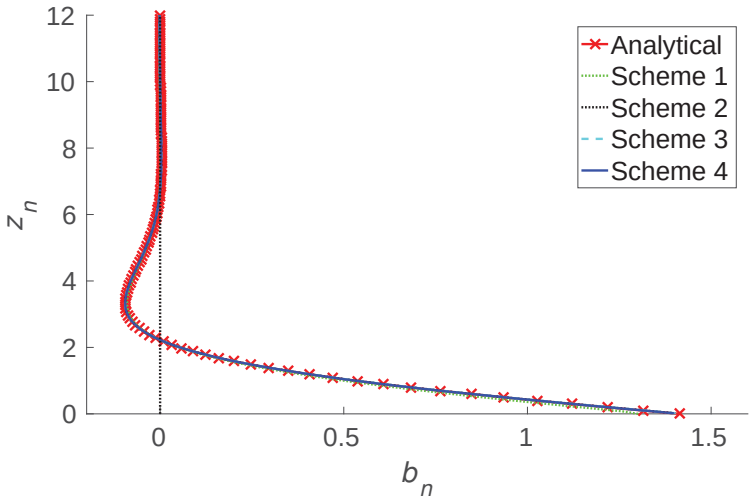

Fig. 4 Normalized buoyancy. Comparison of results from different buoyancy-reconstruction schemes with the analytical solution of the Prandtl model for laminar katabatic flow.

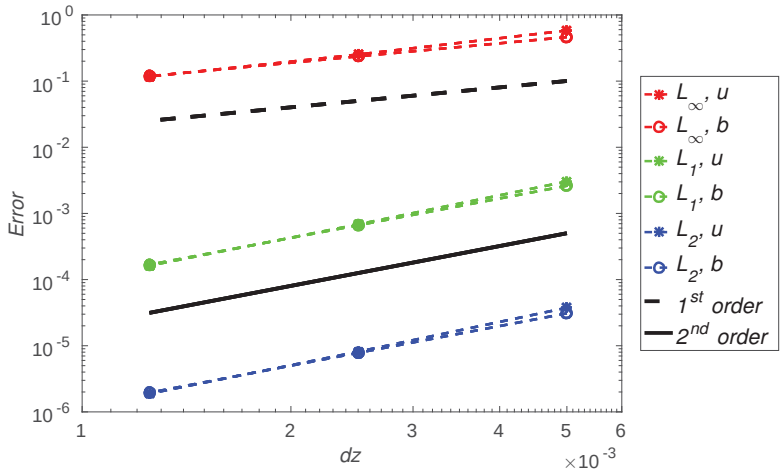

Fig. 5 Study of grid convergence of scheme 4. The L_1 and L_2 norms show second-order accuracy globally for both velocity and buoyancy fields. The L_∞ norm shows first-order accuracy locally at the immersed-boundary node.

the scalar node in the staggered-grid configuration. Relevant flow parameters are given in Table 1. The size of the domain is 0.64 m $\times$ 0.64 m $\times$ 1.6 m in the x-, y- and z-directions, respectively, corresponding to the downslope, cross-slope and slope-normal directions, respectively. Boundary conditions are the same as those for the laminar case (see Sect. 4.1). The grid dimensions are 257 $\times$ 257 $\times$ 641 with uniform spacing of $\Delta = 0.00025$ m. The result-

ing integral slope-flow Reynolds number is $Re_I = 5773$. Given the analog of the Kolmogorov microscale $L_m = \nu^{3/4}|B_s|^{-1/4}$, the resolvability condition for DNS (Pope, 2000) is met by $\Delta \leq 2L_m$.

The immersed-boundary schemes are assessed relative to simulations performed with a body-fitted mesh using the same flow solver. Additionally, a second reference solution from Fedorovich and Gibbs (2015, private communication), and a third reference solution produced by the MicroHH code (van Heerwaarden et al., 2017a) as presented in van Heerwaarden et al. (2017b) are included as additional solutions to the body-fitted mesh for reference to better assess the sensitivities of the simulations to the numerical methods. Figure 6 shows a volume rendering of the instantaneous velocity obtained with DNS, with the mean velocity profiles shown in Fig. 7. Although these schemes agree well with the analytical solution in laminar flow simulations, errors in the peak velocity of the low-level jet are easily detected for schemes 2 and 3 for the turbulent case, validating our hypothesis regarding the inconsistent performance for turbulent flow. Scheme 4 agrees well with the simulation using the body-fitted mesh, and deviates slightly near the upslope return-flow region. As for the laminar case, discrepancies in buoyancy are less apparent in Fig. 8; however, scheme 4 agrees well with the simulation using the body-fitted mesh.

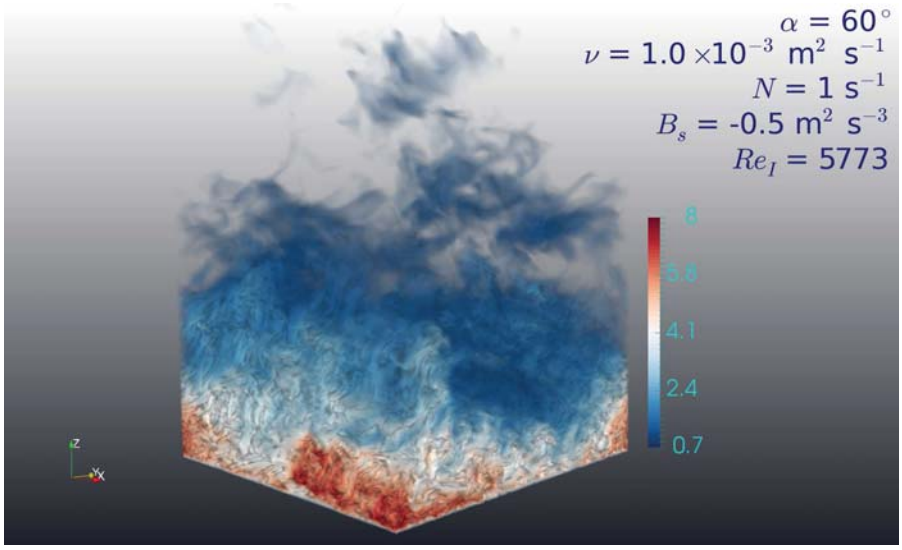

Fig. 6 Three-dimensional volume rendering of instantaneous velocity from direct numerical simulation of the turbulent katabatic flow. The simulation is for an infinite plane inclined at an angle $\alpha = 60^o$. However, the slope is rotated downwards to an isometric view here to enhance the view of turbulence throughout the domain.

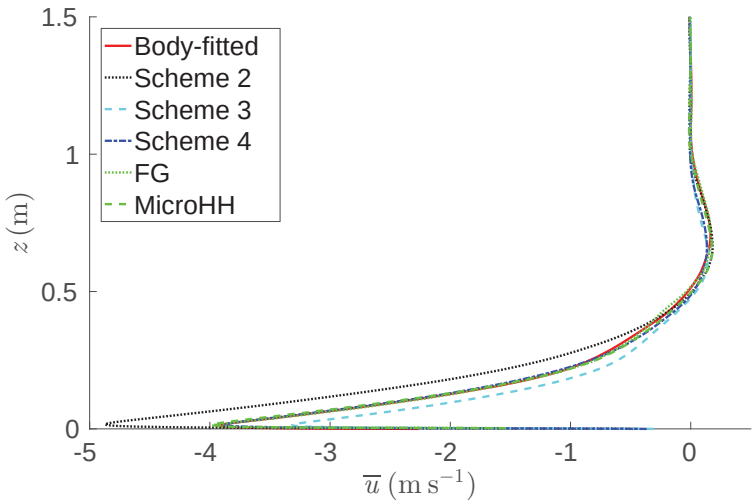

Fig. 7 Downslope velocity in a turbulent katabatic flow. Comparison of immersed-boundary reconstruction scheme with results from three different DNS studies using body-fitted meshes. FG refers to the simulation data presented in Fedorovich and Gibbs (2015, private communication). MicroHH refers to the simulation data presented in van Heerwaarden et al. (2017b)

4.3 Turbulent Katabatic Flow, Second-Order Statistics

Of the three schemes used to simulate a turbulent katabatic slope flow, scheme 4 agrees best with the first-order statistics of the reference solution using a body-fitted mesh. Therefore, only the second-order statistics of scheme 4 are investigated. With respect to the slope-normal buoyancy flux shown in Fig. 9, scheme 4 agrees well with the body-fitted mesh approach, but deviates slightly from the reference solution in the upslope, return-flow region. All four approaches exhibit similar trends with slight variations in this region. The slope-normal momentum flux in Fig. 10 shows a similar variation among the four approaches as well. Scheme 4 agrees best with the reference solution of Fedorovich and Gibbs (2015, private communication) in reproducing the low-level jet, but best with our body-fitted approach in the upslope return flow.

As shown in Fig. 11, variation among the four approaches is the most pronounced, suggesting the downslope velocity variance in the vicinity of the surface is sensitive to the details of the numerical approach. Within and above the region of the upslope return flow, Scheme 4 agrees well with the other approaches. Of the other variances shown in Figs. 12, 13 and 14, all four approaches have excellent agreement among themselves. A critical inspection of scheme 4 reveals the peaks near the surface for cross-slope and slope-normal velocity variances are slightly lower in magnitude compared with the other three DNS approaches. In the cross-slope and slope-normal velocity variances in Figs. 12 and 13, scheme 4 produces the lowest magnitude of variance within

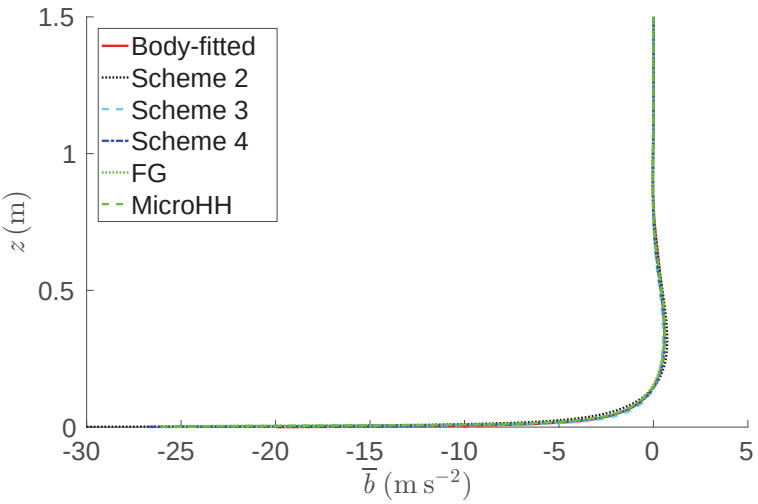

Fig. 8 Buoyancy in a turbulent katabatic flow. Comparison of the immersed-boundary reconstruction scheme with results from three different DNS studies using body-fitted meshes. FG refers to the simulation data presented in Fedorovich and Gibbs (2015, private communication). MicroHH refers to the simulation data presented in van Heerwaarden et al. (2017b)

and above the region of upslope return flow, although this difference from the other three approaches can be assumed negligible. The buoyancy variance in Fig. 14 shows very little variation among the different solutions considered in the present study. Overall, the agreement of scheme 4 with the other three approaches is very good in all the second-order statistics and encourages us to consider it in a future work studying turbulent katabatic flows over complex terrain with heterogeneous surface boundary conditions.

5 Conclusions

We studied the performance of four immersed-boundary reconstruction schemes as a proof-of-concept for imposing a Neumann-type boundary condition on the buoyancy field of an idealized katabatic slope flow. We have shown that the choice of the immersed-boundary reconstruction scheme for Neumann-type boundary conditions has a significant impact on the accuracy of the results. Despite having the same formal order of accuracy globally, second-order turbulence statistics obtained from direct numerical simulations showed significant differences among the schemes considered. Therefore, we suggest validating immersed-boundary reconstruction schemes in both laminar and turbulent flow regimes.

In designing an immersed-boundary reconstruction scheme, we paid particular attention to exclude neighbouring immersed-boundary nodes in the

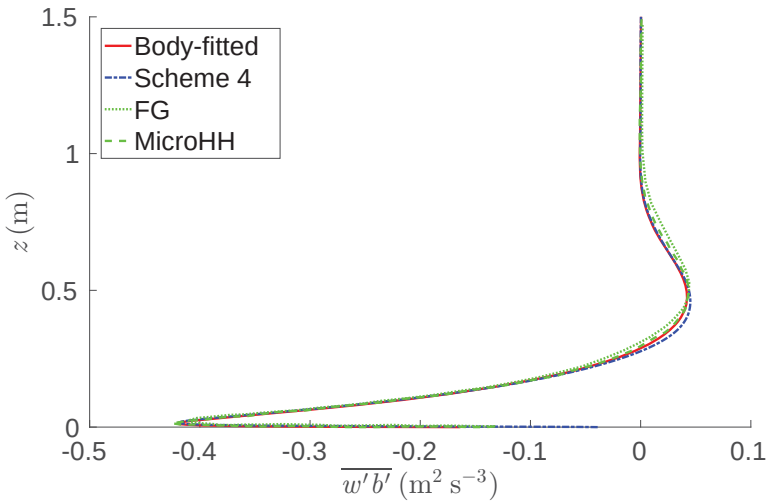

Fig. 9 Slope-normal buoyancy flux in a turbulent katabatic flow. Comparison of immersed-boundary reconstruction scheme 4 with three different DNS studies using body-fitted meshes. FG refers to the simulation data presented in Fedorovich and Gibbs (2015, private communication). MicroHH refers to the simulation data presented in van Heerwaarden et al. (2017b).

reconstruction of a quantity at the immersed-boundary node. We find this subtle issue to be important even for laminar flows. Consequently, we developed a reconstruction scheme (i.e. scheme 4 here) for imposing a Neumann-type boundary condition at an immersed boundary. Scheme 4 performed well in reproducing both the laminar and turbulent flows. First- and second-order turbulence statistics obtained from direct numerical simulations agree well with solutions using a body-fitted mesh. The current simulation over flat terrain constitutes a proof-of-concept, and demonstrates critical issues pertinent to the immersed-boundary method. In future work, we will focus on extending and testing the proposed scheme for complex terrain with heterogeneous surface conditions.

Acknowledgements This material is based upon work supported by the National Science Foundation under Grant No. 1056110 and 1229709. The first author was partially funded by the Idaho Space Grant Consortium (ISGC) through the NASA EPSCoR Graduate Fellowship program. The second author would like to acknowledge the generous support he received through the University of Idaho President's Doctoral Scholars Award. We thank Prof. Evgeni Fedorovich, Dr. Jeremy Gibbs and Dr. Chiel van Heerwaarden for allowing us to use their results for comparison.

References

Cuxart J, Jimnez MA, Martnez D (2007) Nocturnal meso-beta basin and katabatic flows on a midlatitude island. Mon Wea Rev 135(3):918–932

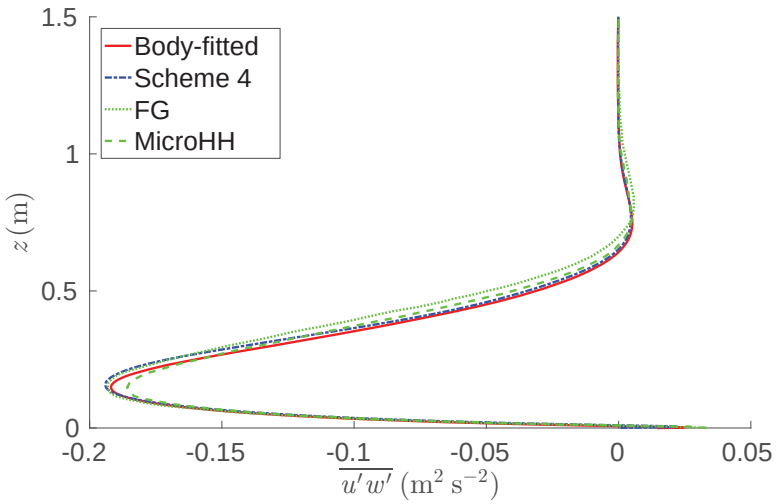

Fig. 10 Slope-normal momentum flux in a turbulent katabatic flow. Comparison of immersed-boundary reconstruction scheme 4 with three different DNS studies using body-fitted meshes. FG refers to the simulation data presented in Fedorovich and Gibbs (2015, private communication). MicroHH refers to the simulation data presented in van Heerwaarden et al. (2017b).

DeLeon R, Felzien K, Senocak I (2012) Toward a GPU-accelerated immersed boundary method for wind forecasting over complex terrain. In: ASME 2012 Fluids Engineering Division Summer Meeting, vol 1, pp 8–12

DeLeon R, Jacobsen D, Senocak I (2013) Large-eddy simulations of turbulent incompressible flows on GPU clusters. Comput Sci Eng 15(1):26–33

Fadlun EA, Verzicco R, Orlandi P, Mohd-Yusof J (2000) Combined immersed-boundary finite-difference methods for three-dimensional complex flow simulations. J Comput Phys 161(1):35–60

Fedorovich E, Shapiro A (2009) Structure of numerically simulated katabatic and anabatic flows along steep slopes. Acta Geophys 57(4):981–1010

Ferziger JH, Perić M (2012) Computational methods for fluid dynamics. Springer Science & Business Media, 426 pp

Gilmanov A, Acharya S (2008) A hybrid immersed boundary and material point method for simulating 3D fluidstructure interaction problems. Int J Numer Meth Fl 56(12):2151–2177

Gilmanov A, Sotiropoulos F (2005) A hybrid Cartesian/immersed boundary method for simulating flows with 3D, geometrically complex, moving bodies. J Comput Phys 207(2):457 – 492

Gilmanov A, Sotiropoulos F, Balaras E (2003) A general reconstruction algorithm for simulating flows with complex 3D immersed boundaries on Cartesian grids. J Comput Phys 191(2):660 – 669

van Heerwaarden C, van Stratum B, Heus T (2017a) microhh/microhh 1.0.0_RC6. https://doi.org/10.5281/zenodo.401381

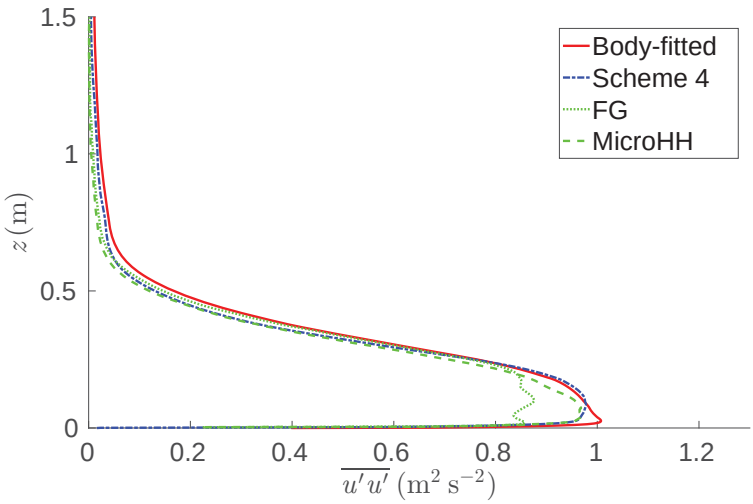

Fig. 11 Down-slope velocity variance in a turbulent katabatic flow. Comparison of immersed-boundary reconstruction scheme 4 with three different DNS studies using body-fitted meshes. FG refers to the simulation data presented in Fedorovich and Gibbs (2015, private communication). MicroHH refers to the simulation data presented in van Heerwaarden et al. (2017b).

van Heerwaarden C, van Stratum B, Heus T, Gibbs J, Fedorovich E, Mellado J (2017b) MicroHH 1.0: a computational fluid dynamics code for direct numerical simulation and large-eddy simulation of atmospheric boundary layer flows. Geosci Model Dev, http://www.geosci-model-dev-discuss.net/gmd-2017-41/

Jacobsen DA, Senocak I (2011) A full-depth amalgamated parallel 3D geometric multigrid solver for GPU clusters. In: 49th AIAA Aerospace Science Meeting

Jacobsen DA, Senocak I (2013) Multi-level parallelism for incompressible flow computations on GPU clusters. Parallel Comput 39(1):1–20

Kang S, Iaccarino G, Ham F (2009) DNS of buoyancy-dominated turbulent flows on a bluff body using the immersed boundary method. J Comput Phys 228(9):3189–3208

Mahrt L (2014) Stably stratified atmospheric boundary layers. Annu Rev Fluid Mech 46(1):23–45

Mahrt L (2016) Stably stratified flow in a shallow valley. Boundary-Layer Meteorol pp 1–20

Mittal R, Iaccarino G (2005) Immersed boundary methods. Annu Rev Fluid Mech 37:239–261

Mohd-Yusof J (1997) Combined immersed-boundary/b-spline methods for simulations of flow in complex geometries. CTR Annual Research Briefs, Center for Turbulence Research, NASA Ames Research Center/ Stanford University pp 317–327

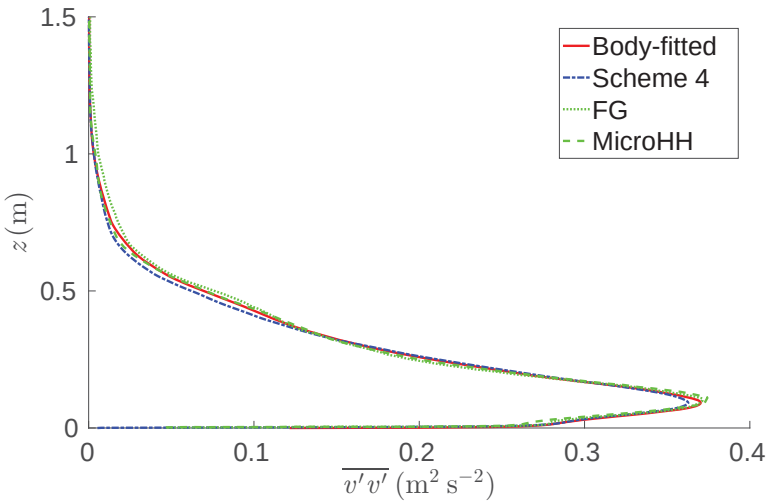

Fig. 12 Cross-slope velocity variance in a turbulent katabatic flow. Comparison of immersed-boundary reconstruction scheme 4 with three different DNS studies using body-fitted meshes. FG refers to the simulation data presented in Fedorovich and Gibbs (2015, private communication). MicroHH refers to the simulation data presented in van Heerwaarden et al. (2017b).

Pacheco-Vega A, Pacheco JR, Rodić T (2007) A general scheme for the boundary conditions in convective and diffusive heat transfer with immersed boundary methods. ASME J Heat Transfer 129(11):1506–1516

Papadopoulos KH, Helmis CG (1999) Evening and morning transition of katabatic flows. Boundary-Layer Meteorol 92(2):195–227

Parish T, Waight III K (1987) The forcing of Antarctic katabatic winds. Mon Wea Rev 115(10):2214–2226

Peskin CS (1972) Flow patterns around heart valves: a numerical method. J Comput Phys 10(2):252–271

Pope SB (2000) Turbulent flows. Cambridge University Press, 806 pp

Prandtl L (1942) Führer durch die Strömungslehre. Vieweg und Sohn, 790 pp

Senocak I, Ackerman AS, Stevens DE, Mansour NN (2004) Topography modeling in atmospheric flows using the immersed boundary method. Annual Research Briefs, Center for Turbulence Research, NASA-Ames/Stanford University

Senocak I, Ackerman AS, Kirkpatrick MP, Stevens DE, Mansour NN (2007) Study of near-surface models for large-eddy simulations of a neutrally stratified atmospheric boundary layer. Boundary-Layer Meteorol 124(3):405–424

Senocak I, Sandusky M, DeLeon R, Wade D, Felzien K, Budnikova M (2015) An immersed boundary geometric preprocessor for arbitrarily complex terrain and geometry. J Atmos Ocean Tech 32(11):2075–2087

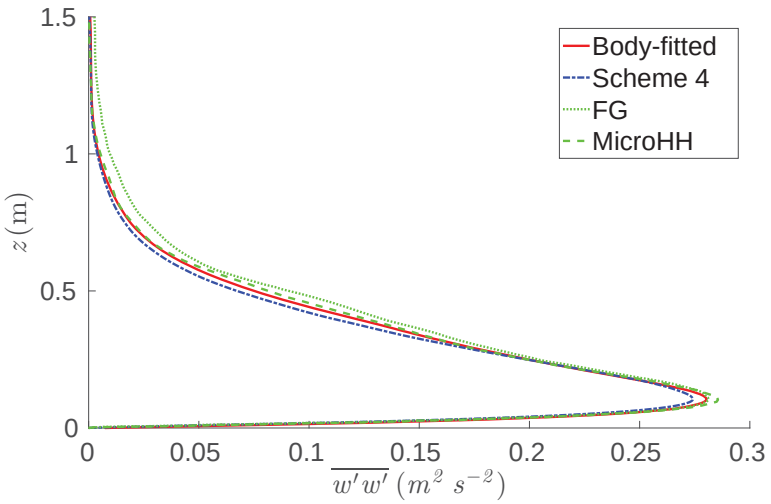

Fig. 13 Slope-normal velocity variance in a turbulent katabatic flow. Comparison of immersed-boundary reconstruction scheme 4 with three different DNS studies using body-fitted meshes. FG refers to the simulation data presented in Fedorovich and Gibbs (2015, private communication). MicroHH refers to the simulation data presented in van Heerwaarden et al. (2017b).

Shapiro A, Fedorovich E (2004) Unsteady convectively driven flow along a vertical plate immersed in a stably stratified fluid. J Fluid Mech 498:333–352

Shapiro A, Fedorovich E (2007) Katabatic flow along a differentially cooled sloping surface. J Fluid Mech 571:149–175

Skyllingstad ED (2003) Large-eddy simulation of katabatic flows. Boundary-Layer Meteorol 106(2):217–243

Smolarkiewicz PK, Sharman R, Weil J, Perry SG, Heist D, Bowker G (2007) Building resolving large-eddy simulations and comparison with wind tunnel experiments. J Comput Phys 227(1):633 – 653

Sotiropoulos F, Yang X (2014) Immersed boundary methods for simulating fluid–structure interaction. Prog Aerosp Sci 65:1–21

Tannehill JC, Anderson D, Pletcher RH (1997) Computational Fluid Mechanics and Heat Transfer, Second Edition. Series in Computational and Physical Processes in Mechanics and Thermal Sciences, Taylor & Francis, 816 pp

Thibault JC, Senocak I (2012) Accelerating incompressible flow computations with a Pthreads-CUDA implementation on small-footprint multi-GPU platforms. J Supercomput 59:693–719

Tseng Y, Ferziger J (2003) A ghost-cell immersed boundary method for flow in complex geometry. J Comput Phys 192(2):593 – 623

Umphrey C, DeLeon R, Senocak I (2016) A Cartesian immersed boundary method to simulate stably stratified turbulent flows. In: 54th AIAA

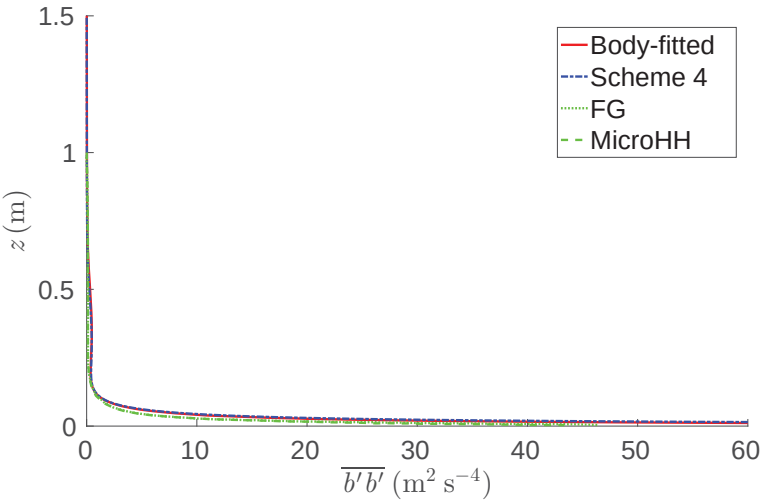

Fig. 14 Buoyancy variance in a turbulent katabatic flow. Comparison of immersed-boundary reconstruction scheme 4 with three different DNS studies using body-fitted meshes. FG refers to the simulation data presented in Fedorovich and Gibbs (2015, private communication). MicroHH refers to the simulation data presented in van Heerwaarden et al. (2017b).

Aerospace Science Meeting

Zhang N, Zheng Z, Eckels S (2008) Study of heat-transfer on the surface of a circular cylinder in flow using an immersed-boundary method. Int J Heat Fluid Fl 29(6):1558–1566